Available online at www.sciencedirect.com
SCIENCE DIRECT®
Journal of Magnetic Resonance 170 (2004) 336–344
JMR Journal of Magnetic Resonance
www.elsevier.com/locate/jmr

Solid-state ^{33}S MAS NMR of inorganic sulfates

Todd A. Wagler, William A. Daunch, Matthew Panzner, Wiley J. Youngs, Peter L. Rinaldi*

Knight Chemical Laboratory, Department of Chemistry, The University of Akron, Akron, OH 44325-3601, USA

Received 6 May 2004; revised 19 July 2004
Available online 23 August 2004

Abstract

Solid-state ^{33}S MAS NMR spectra of a variety of inorganic sulfates have been obtained at magnetic field strengths of 4.7, 14.1, 17.6, and 18.8 T. Some of the difficulties associated with obtaining natural abundance ^{33}S NMR spectra have been overcome by using a high magnetic field strength and magic angle spinning (MAS). Multiple factors were considered when analyzing the spectral linewidths, including magnetic field inhomogeneity, dipolar coupling, chemical shift anisotropy, chemical shift dispersion, and quadrupolar coupling. In most of these sulfate samples, quadrupolar coupling was the dominant line broadening mechanism. Nuclear electric quadrupolar coupling constants (C_q) as large as 2.05 MHz were calculated using spectral simulation software. Spectral information from these new data are compared with X-ray measurements and GAUSSIAN 98W calculations. A general correlation was observed between the magnitude of the C_q and the increasing difference between S–O bond distances within the sulfate groups. Solid-state ^{33}S spin–lattice (T_1) relaxation times were measured and show a significant reduction in T_1 for the hydrated sulfates. This is most likely the result of the modulation of the time-dependent electric field gradient at the nuclear site by motion of water molecules. This information will be useful in future efforts to use ^{33}S NMR in the compositional and structural analysis of sulfur containing materials.

1. Introduction

The only isotope of sulfur detectable by NMR, ^{33}S, happens to be among the first NMR-active nuclei to be studied. In 1951 Dharmatti and Weaver [1] determined the magnetic moment of ^{33}S using the observed signal from a pure sample of CS_2. Unfortunately, since then fewer than 200 scientific papers have been published on ^{33}S NMR, with much of the work focused heavily on sulfur compounds in solution. Most of those solution studies have been performed on S^{IV} and S^{VI} species, which exist in environments with high electronic symmetry around the sulfur nucleus [2–5]. It has only been recently that unsymmetric sulfur species have been studied in solution using high magnetic fields [6,7].

There are very few solid-state ^{33}S NMR studies described in the literature, and they are briefly summarized in the four published reviews of ^{33}S NMR [8–11]. The most comprehensive study to date was published in 1986 [12]. In that work, which was performed with hardware available at the time, the authors examined chemical shifts, linewidths, and second order quadrupolar broadening effects on the static lineshapes of the central ($-1/2 \leftrightarrow +1/2$) transition of a number of sulfur containing inorganic compounds. In the time since this publication, very little new solid-state ^{33}S NMR work has been reported in the literature [13–15].

The dearth of ^{33}S NMR work is rather discouraging, since NMR has proven to be an invaluable tool for most chemists and the fact that sulfur, and more notably sulfate, compounds are important to both the biochemical and chemical industries. Large quantities of sulfates are consumed every year in the manufacturing of wallboard (gypsum), in the tanning and dyeing (alums) industries,

* Corresponding author. Fax: +1 330 972 5256.
E-mail address: PeterRinaldi@uakron.edu (P.L. Rinaldi).

1090-7807/$ - see front matter © 2004 Elsevier Inc. All rights reserved.
doi:10.1016/j.jmr.2004.07.011

and in the petroleum industry. It has also been shown that sulfates play an important role in mediating dissolution and precipitation of potentially toxic contaminants in our environment. Moreover, and probably most important, sulfate is known to be an essential electrolyte which is required for the proper growth and development of living organisms [16].

There are several reasons why so little ^{33}S NMR work has been published. ^{33}S has a small gyromagnetic ratio (1/13 that of ^{1}H) and a low natural abundance (0.75%), making it among the most difficult nuclei to study by NMR. Its receptivity, a measure of the absolute signal strength from a fixed number of nuclei, is 1.7×10^{-5} relative to that of ^{1}H, and 9.72×10^{-2} relative to that of ^{13}C [17]. Furthermore, unlike the more commonly studied ^{1}H and ^{13}C nuclei, ^{33}S is a quadrupolar nucleus with a nuclear spin $I = 3/2$ and a relatively large quadrupole moment ($Q = -0.0678$ b) [18,19]. The large quadrupole moment results in rapid T_2 relaxation leading to extremely broad lines in chemical species having unsymmetrical sulfur environments.

Even with these inherent difficulties, there are very compelling reasons to use ^{33}S NMR. Significant chemical structure information can be obtained by directly observing ^{33}S. Its chemical shift range exceeds 800 ppm, which is approximately four times that of ^{13}C and nearly 16 times that of ^{1}H. Additionally, because sulfur is often directly involved in many of the chemical transformations of interest, its NMR properties are more sensitive than those of nuclei such as ^{1}H and ^{13}C which are only indirectly affected.

Until recently, it has been exceedingly difficult to extract information from the NMR spectra of quadrupolar nuclei like ^{33}S. Fortunately, higher magnetic field strengths and a variety of new experimental techniques can now be used to average the effect of quadrupolar broadening, and improve both sensitivity and resolution [20]. In addition, line narrowing can be attained through partial averaging of the second order quadrupolar interaction using high speed sample rotation at the "magic angle," $\theta = 54.7°$. Theoretical investigations of the quadrupolar spin interaction tensors have shown that complete averaging can be achieved by mechanical means (e.g., dynamic angle spinning [21–24] and double rotation [25,26]), or by pulsed NMR techniques like multiple quantum excitation [27,28].

To determine the degree of resolution and sensitivity enhancement achievable with current instrumental capabilities, this paper compares solid-state ^{33}S NMR spectra of a variety of inorganic sulfates obtained at 4.7, 11.7, 14.1, 17.6, and 18.8 T. Spectral information from this new data are compared with X-ray analysis and GAUSSIAN 98W (G98W) [29] calculations to determine the source of the complex NMR lineshapes observed.

2. Experimental

A variety of inorganic sulfates were obtained from commercial sources, and most were used as received. $(NH_4)_2SO_4$, $NH_4Al(SO_4)_2 \cdot 12H_2O$, K_2SO_4, $KAl(SO_4)_2 \cdot 12H_2O$, and $CsAl(SO_4)_2 \cdot 12H_2O$ were recrystallized from water for X-ray crystallography measurements. For all other samples, space group and unit cell parameters were taken from the literature. Table 1 shows the sample supplier, space group, unit cell parameters and purity of the samples studied. All X-ray data, except for $(NH_4)_2SO_4$, which was studied at 100 and 298 K, were collected at 100 K using MoKα (0.71073 Å) radiation on a Bruker APEX CCD diffraction system. Unit cell parameters were obtained by indexing the peaks of the first 60 frames, and refined using the entire data set. All frames were integrated using the Bruker Saint program, and structures were solved using direct methods. The coordinate data obtained by X-ray crystallography measurements were used in G98W to calculate the electric field gradient around the sulfur nucleus. The Hartree–Fock method with a basis set of 6-311+G(3df) was used in all calculations. G98W calculations were run on a dual processor 2.8 GHz Xeon Gateway PC (note: only one CPU can be utilized with the windows version of G98W).

^{33}S NMR data were collected on a variety of instruments including Varian Unity^{plus} 200, 600, and 750, and Bruker AMX 800 MHz spectrometers operating at 4.7, 14.1, 17.6, and 18.8 T, respectively. Samples were ground and packed as powders into silicon nitride or zirconia ceramic rotors and sealed with Kel-F, Vespel, or Aurum end caps. All samples underwent MAS with rates ranging from 6 to 10 kHz. A Doty Scientific, wide bore, broadband MAS probe, optimized for observing ^{13}C at 4.7 T was tuned to the lower ^{33}S resonance frequency by adding additional capacitance to the probes X channel tuning circuit. A second Doty Scientific, narrow bore, MAS probe was optimized in a similar fashion for experiments performed at 14.1 T. A Varian/Chemagnetics T3 two channel probe, optimized for observing ^{33}S, was used with a Unity^{plus} 750 MHz (17.6 T) spectrometer. One Bruker, single-channel probe, optimized for observing low frequencies was employed at 18.8 T.

Magnetic field homogeneity was adjusted by shimming on the deuterium or proton signal from 99% D_2O. At 4.7 and 17.6 T the ^{1}H linewidths at half height from the residual HDO were 4 and 12 Hz, respectively. The B_0 field inhomogeneity contribution to the ^{33}S linewidth was estimated to be $\leqslant 1$ Hz. Chemical shift referencing and 90° pulse widths were determined using primary and secondary ^{33}S standards. ^{33}S signals were referenced relative to external 1 M aqueous Cs_2SO_4 (at 333 ppm relative to CS_2). The 90° pulse widths were determined using either 1 M aqueous Cs_2SO_4 or solid CaS (cubic symmetry), both samples gave the same

Table 1
Inorganic sulfate compounds studied

Compound	Supplier	Space group	a (Å)	b (Å)	c (Å)	Ref.	Purity
Na_2SO_4	Aldrich	Fddd	9.829	12.302	5.868	[44]	99.99%
$(NH_4)_2SO_4$	Aldrich		7.747	10.593	5.977	[45]	99.99%
at 100 K		$Pna2_1$	7.8932(13)	10.5080(18)	5.9364(10)	—[b]	
at 298 K		Pnma	7.709(4)	5.940(3)	10.532(5)	—[b]	
$NH_4Al(SO_4)_2 \cdot 12H_2O$	Aldrich	$Pa\bar{3}$	12.248	12.248	12.248	[46]	99.99%
			12.2281(4)	12.2281(4)	12.2281(4)	—[b]	
K_2SO_4	Fisher Sci.	Pnma	7.476	5.763	10.07	[47]	Reagent grade
			7.4256(11)	5.7317(8)	10.0031(15)	—[b]	
$KAl(SO_4)_2 \cdot 12H_2O$	Mallinckrodt	$Pa\bar{3}$	12.157	12.157	12.157	[48]	Reagent grade
			12.1136(4)	12.1136(4)	12.1136(4)	—[b]	
Rb_2SO_4	Pfaltz and Bauer	Pnma	7.814	10.422	5.975	[49]	Technical grade
Cs_2SO_4	Aldrich	Pnma	8.239	10.937	6.256	[49]	99.99%
$CsAl(SO_4)_2 \cdot 12H_2O$	Aldrich	$Pa\bar{3}$	12.3019(3)	12.3019(3)	12.3019(3)	—[b]	99.99%
$MgSO_4$	EM Science	Rhombic	4.82	6.72	8.35	[50]	>98%
$MgSO_4 \cdot 6H_2O$	—[a]	C2/c	10.0014(7)	7.2077(5)	24.2810(18)	—[b]	
$CaSO_4$	Aldrich	Amma	6.993	6.995	6.245	[51]	99%
$CaSO_4 \cdot 2H_2O$	Aldrich	I2/c	5.679	15.202	6.522	[52]	98%
$BaSO_4$	Aldrich	Pbnm	7.154	8.879	5.454	[40]	99%
		Pnma	8.884(4)	5.458(3)	7.153(3)	[41]	

[a] $MgSO_4$ recrystallized from water.
[b] X-ray data obtained in-house.

result. Typical 90° (liquid) pulse width values were 5 and 8 μs at 17.6 and 4.7 T, respectively.

A one-pulse experiment was used at 17.6 T to obtain spectra for chemical shift and linewidth measurements. Because a baseline roll from acoustic probe ringing was observed at low field, the ring down elimination (RIDE) pulse sequence [10] was used to acquire spectra at 4.7 T for those samples that gave broad resonances. Spin–lattice relaxation (T_1) measurements were obtained using the inversion recovery sequence (delay–π–τ–π/2–acquire). The Varian STARS software package [30–32] was used to determine the relative magnitude of the quadrupole coupling constant (C_q), asymmetry parameter (η_q), and chemical shift. Lineshape simulations were performed on a Sun Ultra Sparc workstation.

3. Results and discussion

Typically solid-state ^{33}S NMR spectral linewidths are dominated by the broadening from quadrupolar interactions. In the solid state, the outer ($-3/2 \leftrightarrow -1/2$ and $+1/2 \leftrightarrow +3/2$) spectral transitions are usually broadened beyond detection by quadrupolar interactions. However, the central ($-1/2 \leftrightarrow +1/2$) transition, to a first approximation, is unaffected by these same interactions and can produce relatively narrow resonances. In cases where the quadrupolar interaction is comparable to the resonance frequency (e.g., in unsymmetrical structures), second order quadrupolar effects can lead to significant broadening of the central transition. For quadrupolar broadened resonances the spectral linewidth is inversely proportional to the strength of the applied magnetic field. Therefore, the spectral linewidth can be reduced by using a stronger magnetic field.

The benefits of using a high magnetic field, including improved sensitivity and resolution, are illustrated in Fig. 1 which shows spectra of $KAl(SO_4)_2 \cdot 12H_2O$ obtained at 4.7 and 17.6 T. The spectrum shown in Fig. 1A required 2 days of signal averaging at 4.7 T using a 7 mm rotor with a 215 μl sample volume. However, only 1 h of signal averaging was needed at 17.6 T to acquire an adequate spectrum using a 5 mm rotor with a 90 μl sample volume. Another benefit of using a high magnetic field strength was the reduction of acoustic ringing.

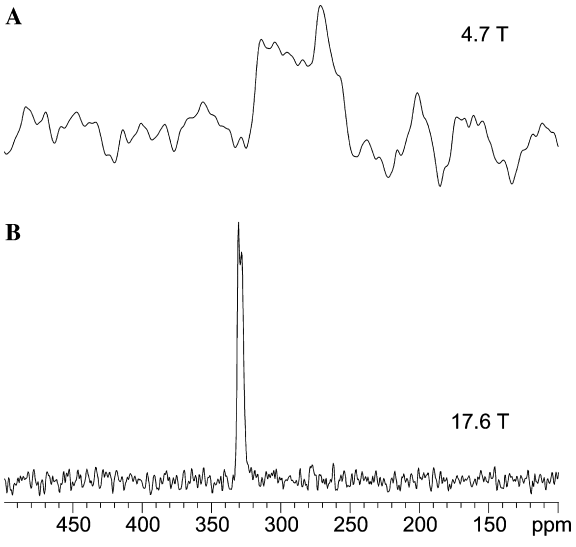

Fig. 1. Solid-state ^{33}S MAS NMR spectra of $KAl(SO_4)_2 \cdot 12H_2O$: (A) acquired at 4.7 T in 2 days; and (B) acquired at 17.6 T in 1 h.

Several contributions were considered when analyzing the ^{33}S NMR spectral linewidths, including: dipolar coupling, magnetic field inhomogeneity, chemical shift anisotropy (CSA), chemical shift dispersion (CSD), and quadrupolar coupling. Dipolar coupling is dependent on the internuclear distance and the gyromagnetic ratios ($\gamma_I\gamma_S\hbar/r^3$) of the interacting nuclei. Most of the NMR active nuclei under consideration have a small gyromagnetic ratio. ^{33}S has a gyromagnetic ratio of 2.055685×10^7 rad/T s. Therefore, the dipolar couplings are expected to be small and are effectively averaged by MAS, even at modest spin rates of a few kHz. Magnetic field inhomogeneity was also found to be small, and contributes $\leqslant 1$ Hz to the width of the ^{33}S resonances. Spinning at frequencies greater than the static linewidth will eliminate broadening from CSA, dipolar coupling, and first order quadrupolar coupling. Therefore, second order quadrupolar coupling and CSD (from variations in sample morphology) must be the dominant factors influencing linewidth. The linewidth contribution from CSD is proportional to the magnetic field strength [33]. Thus, a fourfold increase in field strength will result in a corresponding increase in CSD contributions to the linewidth. The quadrupolar coupling's contribution to the spectral linewidth is a function of the C_q and the magnetic field strength, defined by [34–36]

$$A = \frac{C_q^2}{\nu_z} \cdot C_I, \tag{1}$$

where $C_I = 3/64$ for $I = 3/2$ and $\nu_z = \frac{\gamma B_0}{2\pi}$. Thus, increasing the field strength should result in a proportional decrease in linewidth if quadrupolar coupling is the primary contributor.

Table 2 summarizes the linewidths measured in this work and for which solid-state ^{33}S NMR data have appeared in the literature. As mentioned above, increasing the field strength should result in a proportional decrease in linewidth if quadrupolar coupling is the dominant line broadening mechanism. This phenomenon is clearly seen in the ^{33}S spectral linewidths of $KAl(SO_4)_2 \cdot 12H_2O$ obtained at 4.7, 11.7, 14.1 17.6, and 18.8 T (Table 2, row 5). Na_2SO_4 and $BaSO_4$ show a similar effect. The decrease in linewidth between the static and MAS spectra, even at low fields, shows that MAS has essentially eliminated the broadening due to dipolar coupling and CSA. In most cases, approximately an order of magnitude reduction in linewidths were observed when comparing the ^{33}S NMR spectra measured from static samples at 11.7 T [12], with the spectra measured at 17.6 T with MAS. For $NH_4Al(SO_4)_2 \cdot 12H_2O$ the linewidth actually increases with increasing field strength (Table 2, row 3). This is similar to the effect seen in symmetric metal sulfides studied earlier, where it was shown that CSD was the dominant line broadening mechanism [15]. Cs_2SO_4 and $(NH_4)_2SO_4$ show a combined influence from both CSD and C_q. For those samples that gave linewidths greater than about 300 Hz at 17.6 T it was not possible to obtain spectra at 4.7 T, even after signal averaging for several days. Time constraints and instrument availability prevented some measurements at 4.7 and 14.1 T.

Fig. 2 shows the 57.6 MHz ^{33}S NMR spectra of several inorganic sulfates. Most of these spectra show features characteristic of second order quadrupolar broadening effects. This is consistent with an unsymmetrical electronic environment around sulfur in these compounds (see Tables 1 and 4). For many sulfur compounds, complete averaging of the second order quadrupolar interaction would require sample spinning around two different axes or special pulse sequences. However, MAS at very high field provided adequate line narrowing to obtain relatively good spectra in a reasonable amount of time. By using high magnetic fields, significant gains in sensitivity and resolution are achieved.

Table 3 compares the chemical shifts and quadrupolar coupling constants obtained at 17.6 T (with MAS)

Table 2
Summary of ^{33}S NMR linewidth data

Compound	$\nu_{1/2}$ (Hz) at 11.7 T Static[a]	$\nu_{1/2}$ (Hz) at 4.7 T MAS = 6 kHz	$\nu_{1/2}$ (Hz) at 14.1 T MAS = 10 kHz	$\nu_{1/2}$ (Hz) at 17.6 T MAS = 6 kHz	$\nu_{1/2}$ (Hz) at 18.8 T MAS = 10 kHz
Na_2SO_4	2300		310	240	
$(NH_4)_2SO_4$	1200	600	140	145	
$NH_4Al(SO_4)_2 \cdot 12H_2O$	950	12	18	18	
K_2SO_4	4300			600	
$KAl(SO_4)_2 \cdot 12H_2O$	2100	850	270	220	210
Rb_2SO_4	3500			500	
Cs_2SO_4	3200		460	400	
$CsAl(SO_4)_2 \cdot 12H_2O$	950			50	
$MgSO_4$	—			2200	
$MgSO_4 \cdot 6H_2O$	—			450	
$CaSO_4$	3500			500	
$CaSO_4 \cdot 2H_2O$	2000			105	
$BaSO_4$	18000		2250	1600	1600

[a] Data obtained from [12].

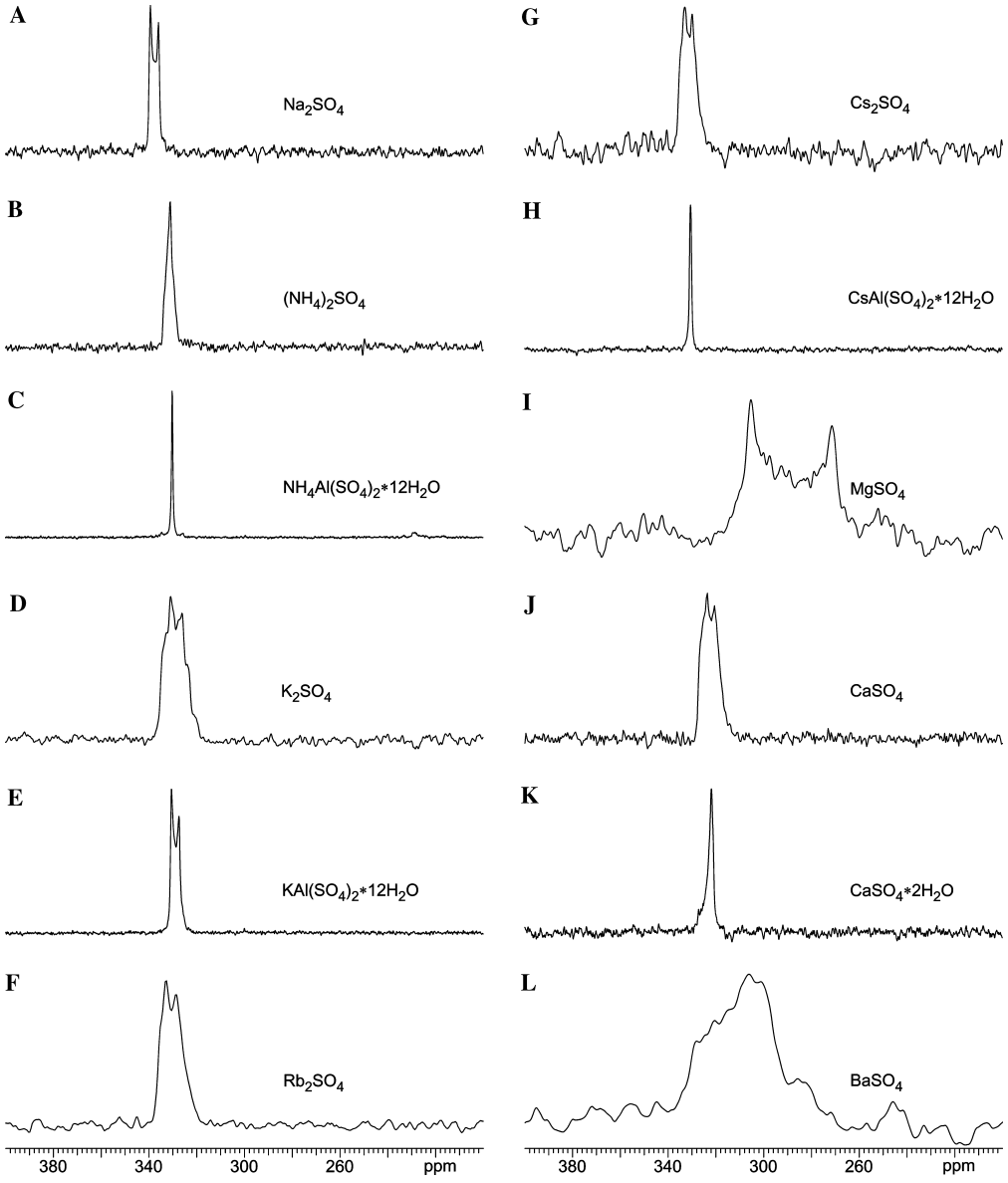

Fig. 2. Solid-state ^{33}S MAS NMR spectra obtained at 57.6 MHz (17.6 T) of the following samples: (A) Na_2SO_4, 30° pulse width, 0.2 s relaxation delay, 214 k scans, 17.5 h; (B) $(NH_4)_2SO_4$, 20° pulse width, 0.3 s relaxation delay, 262 k scans, 24 h; (C) $NH_4Al(SO_4)_2 \cdot 12H_2O$, 45° pulse width, 1.0 s relaxation delay, 44 k scans, 13 h; (D) K_2SO_4, 15° pulse width, 0.5 s relaxation delay, 348 k scans, 53 h; (E) $KAl(SO_4)_2 \cdot 12H_2O$, 90° pulse width, 0.1 s relaxation delay 268 k scans, 11 h; (F) Rb_2SO_4 15° pulse width, 0.2 s relaxation delay, 377 k scans, 24 h; (G) Cs_2SO_4, 45° pulse width, 0.5 s relaxation delay, 65 k scans, 11 h; (H) $CsAl(SO_4)_2 \cdot 12H_2O$, 15° pulse width, 0.5 s relaxation delay, 122 k scans, 20 h; (I) $MgSO_4$, 30° pulse width, 0.2 s relaxation delay, 262 k scans, 21 h; (J) $CaSO_4$, 10° pulse width, 0.04 s relaxation delay, 1491 k scans, 21 h; (K) $CaSO4 \cdot 2H_2O$, 30° pulse width, 0.5 s relaxation delay, 131 k scans, 22 h; and (L) $BaSO_4$, 30° pulse width, 0.2 s relaxation delay, 262 k scans, 18 h. The liquid 90° pulse width was 5.5 μs.

with literature values obtained at 11.7 T (without MAS). In all cases, the quadrupolar coupling constants obtained at 17.6 T are lower than those obtained at 11.7 T. As noted in [12], quadrupolar coupling constants obtained without MAS are to be considered approximate values, since CSA and dipolar coupling also contribute to the linewidths in spectra from static samples. Table 3 also shows the η_q and T_1's obtained at 17.6 T. Due to much lower sensitivity, it was not possible to perform relaxation experiments for most of the samples at 4.7 T. Although a complete understanding of the spin–lattice relaxation behavior would require temperature- or field-dependent spin–lattice relaxation studies, some conclusions can be made from the data provided. For instance, the T_1's of the hydrated samples are significantly lower than the anhydrous samples. This is attributed to the motion of the water molecules in the crystal lattice, which increases the T_1 relaxation efficiency. Haase et al. [37–39] showed that relaxation of ^{27}Al nuclei in hydrated zeolites were overwhelmingly dominated by modulation of the time-dependent electric field gradient at the nuclear site

Table 3
Summary of NMR parameters and $\Delta(S–O)_m$

Compound	δ (ppm) 11.7 T[a]	δ (ppm) 17.6 T	C_q (MHz) 11.7 T[a]	C_q (MHz) 17.6 T[b]	C_q (MHz) G98W	η_q 17.6 T[b]	$\Delta(S–O)_m$ (Å)	T_1 (s)
Na_2SO_4	330	341	0.82	0.66		0.13		30
$(NH_4)_2SO_4$	328	332	0.59	0.58	0.56 at 298 K	0.75	0.008	1
					0.84 at 100 K		0.020	
$NH_4Al(SO_4)_2 \cdot 12H_2O$	333	331	0.53	[c]	0.08	[c]	0.001	0.27
K_2SO_4	334	336	1.13	0.97	0.76	0.50	0.015	16
$KAl(SO_4)_2 \cdot 12H_2O$	327	332	0.79	0.64	0.26 (78%)	0.16	0.004	0.03
					3.08 (22%)		0.060	
Rb_2SO_4	329	337	1.01	0.93		0.42		29
Cs_2SO_4	335	336	0.97	0.83		0.46		16
$CsAl(SO_4)_2 \cdot 12H_2O$	331	330	0.53	0.29	0.29	0.55	0.005	8
$MgSO_4$		325		2.05		0.10		
$MgSO_4 \cdot 6H_2O$		331		0.89	0.70	0.24	0.015	1.4
$CaSO_4$	326	327	1.0	0.90		0.40		45
$CaSO_4 \cdot 2H_2O$	337	327	0.77	0.70		1.00		12
$BaSO_4$		328	2.3	1.70	1.75	0.72	0.034[d]	
					2.87		0.070[e]	

[a] Data obtained from [12].
[b] Determined using Varian STARS lineshape simulation package.
[c] C_q is very small. Unable to determine using STARS.
[d] Determined from [40,42].
[e] Determined from [41,42].

due to motion of water molecules and hydrated cations in zeolite pores. There was no relationship observed between the quadrupole coupling constant and T_1's in the anhydrous samples. This could be a result of impurities within the crystal lattice or structural point defects which can enhance relaxation.

To gain a better understanding of the factors contributing to the lineshapes observed in the spectra of these compounds, six samples were chosen for X-ray crystallography and G98W studies. Table 4 shows S–O bond distances and bond angles for the six compounds studied by X-ray crystallography in our lab, and 2 structures of $BaSO_4$ found in the literature [40–42]. X-ray analysis of the six compounds showed that $(NH_4)_2SO_4$, $NH_4Al(SO_4)_2 \cdot 12H_2O$, K_2SO_4, $CsAl(SO_4)_2 \cdot 12H_2O$, $MgSO_4 \cdot 6H_2O$, and $BaSO_4$ have sulfate groups that are equivalent within their respective unit cells. However, the X-ray data obtained for $KAl(SO_4)_2 \cdot 12H_2O$ revealed that within the orthorhombic crystal lattice, the sulfate groups are disordered and distribute themselves into two separate arrangements. Most of the sulfates (78%) have their oxygen atoms more symmetrically arranged around the central sulfur atom than the second arrangement of sulfates (see Table 4), which include only 22% of the structures. This data indicates that the ^{33}S NMR spectrum of $KAl(SO_4)_2 \cdot 12H_2O$ may actually contain two distinct resonances (see Fig. 2E).

In an attempt to determine if two overlapping resonances were present in the NMR spectrum of $KAl(SO_4)_2 \cdot 12H_2O$, solid-state ^{33}S NMR data at an even higher magnetic field strength was collected. Comparison of the spectra obtained at 4.7 and 18.8 T revealed that no further chemical shift resolution could be observed and that the pattern only appeared to narrow with increasing field strength (see Table 2, row 5). The overall linewidth decreased by a factor of four, as expected from the diminished second order quadrupolar effects at increased field strength. This signifies that the observable pattern is solely due to second order quadrupolar broadening, and that any chemical shift information is either obscured by this pattern or the second resonance is so broad that it is not detected.

S–O bond distances and bond angles of the sulfate groups measured experimentally by X-ray crystallography were directly entered into G98W to calculate the EFG tensors. C_q's were calculated using the largest traceless value of the EFG, given by

$$C_q(\text{MHz}) = 234.96Q(\text{b})q_{zz}(\text{a.u.}), \quad (2)$$

where $Q = -0.0678$ b and q_{zz} = largest traceless value of the EFG. Unfortunately, it was too computationally expensive to simulate a large crystal unit where a centralized sulfate is coordinated to an inner sphere of cations, which in turn are coordinated to a second sphere of sulfate groups. However, the most significant contribution to the asymmetric EFG around the sulfur nucleus is provided by the closest atoms, and a general correspondence can be seen between the calculated and experimentally determined C_q's shown in Table 3, column 5 and 6. In all cases, except $KAl(SO_4)_2 \cdot 12H_2O$, the calculated C_q's are within 25% of the experimentally determined values.

Table 4
Bond distances and bond angles of selected sulfates

Bond distance and bond angle	$(NH_4)_2SO_4$		$NH_4Al(SO_4)_2 \cdot 12H_2O$	K_2SO_4	$KAl(SO_4)_2 \cdot 12H_2O$		$CsAl(SO_4)_2 \cdot 12H_2O$	$MgSO_4 \cdot 6H_2O$	$BaSO_4$[a]	$BaSO_4$[b]
	298 K	100 K			78%	22%				
S–O(1)	1.443(3)	1.4657(14)	1.4727(16)	1.4676(19)	1.470(2)	1.433(7)	1.473(3)	1.4687(9)	1.456(3)	1.472
S–O(2)	1.4472(17)	1.4787(15)	1.4727(16)	1.4809(13)	1.4743(13)	1.493(4)	1.4781(13)	1.4778(9)	1.467(2)	1.448
S–O(3)	1.4472(17)	1.4824(16)	1.4727(16)	1.4809(13)	1.4743(13)	1.493(4)	1.4781(13)	1.4806(9)	1.490(2)	1.518
S–O(4)	1.451(3)	1.4854(13)	1.474(3)	1.4829(18)	1.4743(13)	1.493(4)	1.4781(13)	1.4837(9)	1.490(2)	1.518
∠O(1)–S–O(2)	108.83(10)	109.75(9)	109.61(8)	109.83(7)	109.56(6)	111.14(17)	109.76(6)	110.32(5)	112.3(4)	111.8
∠O(1)–S–O(3)	108.83(10)	110.17(9)	109.61(8)	109.83(7)	109.56(6)	111.14(17)	109.76(6)	109.88(5)	109.7(2)	110.3
∠O(2)–S–O(3)	110.47(15)	108.87(9)	109.61(8)	109.38(11)	109.39(6)	107.75(18)	109.18(6)	109.74(5)	108.6(2)	109.7
∠O(1)–S–O(4)	110.30(17)	110.23(8)	109.33(8)	110.44(11)	109.56(6)	111.14(17)	109.76(6)	109.91(6)	109.7(2)	110.3
∠O(2)–S–O(4)	109.20(10)	108.97(9)	109.33(8)	108.67(7)	109.39(6)	107.75(18)	109.18(6)	108.50(5)	108.6(2)	109.7
∠O(3)–S–O(4)	109.20(10)	108.82(9)	109.33(8)	108.67(7)	109.39(6)	107.75(18)	109.18(6)	108.45(5)	107.8(4)	104.7

[a] Data obtained from [40,42].
[b] Data obtained from [41,42].

Close inspection of the X-ray crystallography data revealed that a correlation existed between the S–O bond distances, d(S–O), and C_q. It was observed that as the disparity in S–O bond distances within the sulfate group grew, the C_q also became larger. The disparity in d(S–O) was characterized best by the difference between the largest and smallest S–O bond distances, given by

$$\Delta(SO)_m = d(SO)_l - d(SO)_s \quad (3)$$

where $d(S–O)_l$ is the longest S–O bond distance and $d(S–O)_s$ is the shortest S–O bond distance within the sulfate group. Fig. 3 shows a plot of C_q vs. $\Delta(S–O)_m$ where the open circles (○) represent the C_q's determined by simulation of the NMR spectra, and the open squares (□) represent the C_q's determined by ab initio calculations. A linear regression fit of the calculated values gave $C_q = 44.0 \times \Delta(S–O)_m + 0.1$. This fit can be used as a predictive tool for optimizing NMR acquisition parameters if X-ray data is available. Table 3 and Fig. 3 show $\Delta(S–O)_m$ for two $BaSO_4$ crystal structures found in the literature [40,41]. This data shows that the $BaSO_4$ sample more closely resembles the Pbnm structure of the material studied by Jacobsen et al. [40].

The two sulfate arrangements in $KAl(SO_4)_2 \cdot 12H_2O$ have a $\Delta(S–O)_m$ of 0.004 Å for the major (78%) form and 0.060 Å for the minor (22%) form of the sulfate groups. This leads to a calculated C_q of 0.26 MHz for sulfate groups of the major component and 3.08 MHz for sulfate groups of the minor component in $KAl(SO_4)_2 \cdot 12H_2O$. Thus, it is highly probable that 22% of the sulfate groups in $KAl(SO_4)_2 \cdot 12H_2O$ are not detected by NMR even at 18.8 T. The large C_q and lower abundance of that sulfate structure reduces the intensity and broadens the resonance so that it is buried in the baseline. Spectral simulation of a two component system, having 78% sulfate groups with a $C_q = 0.64$ MHz and $\eta_q = 0.16$ and 22% sulfate groups with a $C_q = 3.08$

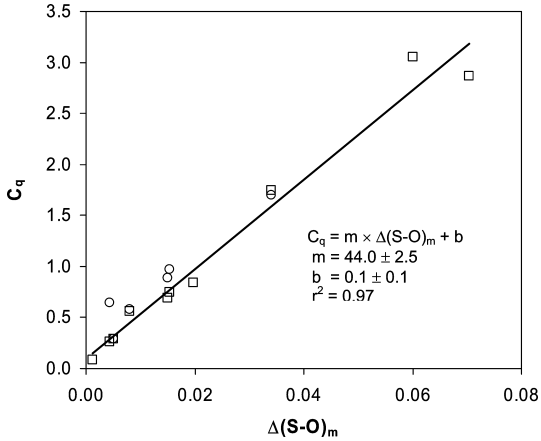

Fig. 3. Plot of C_q vs. $\Delta(S–O)_m$. The open circles (○) are based on the C_q's determined by simulation of the NMR spectra, and the open squares (□) are based on the C_q's calculated by G98W.

and $\eta_q = 0.16$, did indeed show a broad signal from the minor component which was about 50 times weaker than the signal from the major component.

All X-ray crystallography measurements were run at 100 K to reduce thermal motion and to obtain higher resolution. However, it was found that $(NH_4)_2SO_4$ exhibits a phase change at reduced temperature. Ahmed et. al. [43] showed that the lattice parameters and unit cell volume of $(NH_4)_2SO_4$ change as a function of temperature and that it undergoes a transition from a paraelectric phase to a ferroelectric phase at 223 K. Thus, it was necessary to repeat the X-ray crystallography measurements under the same conditions as the NMR experiments. Columns 2 and 3 of Table 4 contain the S–O bond distances and bond angles of $(NH_4)_2SO_4$ obtained at 298 and 100 K. It shows that the $\Delta(S–O)_m$ at 100 K is 0.013 Å resulting in a calculated C_q of 0.84 MHz (see Table 3). At 298 K the $\Delta(S–O)_m$ is only 0.004 Å which leads to a significantly smaller C_q of 0.56 MHz, which is much closer to the experimentally determined value of 0.58 MHz.

4. Conclusions

Solid-state ^{33}S NMR has been largely neglected over the past 50 years mostly because of the difficulty associated with collecting suitable spectra. However, with the increasing number of high field NMR spectrometers available, it should be easier to obtain such spectra. Enormous gains in sensitivity and resolution can be achieved by collecting ^{33}S NMR spectra at a high magnetic field strength. An order of magnitude reduction in linewidth was observed between static spectra obtained at 11.7 T and MAS spectra obtained at 17.6 T, with a concomitant increase in peak height and signal-to-noise. Furthermore, spectra obtained at high fields (high frequencies) lacked acoustic ringing that complicated lower field measurements. Spin–lattice relaxation measurements showed significantly reduced T_1's for the hydrated samples. This resulted from the modulation of the time-dependent electric field gradient at the nuclear site due to motion of water molecules. G98W calculations and X-ray measurements proved helpful in understanding the complex NMR lineshapes of these samples. These techniques also revealed a general correlation between $\Delta(S–O)_m$ and C_q that may be helpful in future studies of sulfates.

Acknowledgments

The authors would like to thank Ann Bolek for her efforts in obtaining much of the crystal structure literature, Simon Stakleff for maintaining the NMR equipment used, the Kresge Foundation and the donors to the Kresge Challenge Program at the University of Akron for funds to purchase the NMR instruments used in this work, and partial support of this research by the Petroleum Research Fund administered by the American Chemical Society (26776-AC). We also wish to thank H. Foerster of Bruker Instruments, B. Bluemich, and the staff of the NMR lab at RWTH, Aachen for assistance in obtaining 800 MHz data.

References

[1] S.S. Dharmatti, H.E. Weaver, Magnetic moment of sulfur-33, Phys. Rev. 83 (1951) 845.
[2] R. Musio, O. Sciacovelli, Detection of taurine in biological tissues by ^{33}S NMR spectroscopy, J. Magn Reson. 153 (2) (2001) 259–261.
[3] R. Gawinecki, E. Kolehmainen, A. Zakrzewski, K. Laihia, B. Osmialowski, R. Kauppinen, Predominance of inductive overresonance substituent effect on ^{33}S NMR chemical shifts of 4-substituted phenyl-4′-methylphenacyl sulfones, Magn. Reson. Chem. 37 (6) (1999) 437–440.
[4] B. Berke, C. Cheze, J. Vercauteren, G. Deffieux, Bisulfite addition to anthocyanins: revisited structures of colorless adducts, Tetrahedron Lett. 39 (32) (1998) 5771–5774.
[5] R. Musio, O. Sciacovelli, ^{33}S NMR Spectroscopy. 2. Substituent effects on ^{33}S chemical shifts and nuclear quadrupole coupling constants in 3- and 4-substituted benzenesulfonates. Correlation between chemical shifts and nuclear quadrupole coupling constants, J. Org. Chem. 62 (26) (1997) 9031–9033.
[6] A. Perjessy, E. Kolehmainen, W.M.F. Fabian, M. Ludwig, K. Laihia, J. Kulhanek, Z. Sustekova, Structure-reactivity-spectra correlations for substituted benzenesulfonamides, Sulfur Lett. 25 (2) (2002) 71–78.
[7] R.A. Aitken, S. Arumugam, S.T.E. Mesher, F.G. Riddell, Natural abundance ^{33}S NMR spectroscopy. The first spectra of several major compound types, J. Chem. Soc. Perkin Trans. 2 (2) (2002) 225–226.
[8] V.M. Bzhezovsky, G.A. Kalabin, Chemistry of Organosulfur Compounds, Horwood, Chichester, 1990.
[9] J.F. Hinton, Sulfur-33 NMR spectroscopy, Annu. Rep. NMR Spectrosc. 19 (1987) 1–34.
[10] P.S. Belton, I.J. Cox, R.K. Harris, Experimental sulfur-33 nuclear magnetic resonance spectroscopy, J. Chem. Soc. Faraday Trans. 2 (81) (1985) 63.
[11] G. Barbarella, Sulfur-33 NMR, Prog. NMR Spectrosc. 25 (1993) 317.
[12] H. Eckert, J.P. Yesinowski, Sulfur-33 NMR at natural abundance in solids, J. Am. Chem. Soc. 108 (1986) 2140.
[13] T.J. Bastow, NMR study of the II-VI semiconductors ZnX (X = O, S, Se, Te), Mater. Australas. 19 (1987) 12.
[14] T.J. Bastow, S.N. Stuart, NMR study of the zinc chalcogenides (ZnX, X = O, S, Se, Te), Phys. Status Solidi B 145 (1988) 719.
[15] T.A. Wagler, W.A. Daunch, P.L. Rinaldi, A.R. Palmer, Solid state ^{33}S NMR of inorganic sulfides, J. Magn. Reson. 161 (2) (2003) 191.
[16] D. Markovich, Physiological roles and regulation of mammalian sulfate transporters, Physiol. Rev. 81 (4) (2001) 1499.
[17] C. Brevard, P. Granger, Handbook of High Resolution Multinuclear NMR, Wiley, New York, 1981.
[18] P. Pyykko, The nuclear quadrupole moments of the 20 first elements: high-precision calculations on atoms and small molecules, Z. Naturforsch. A: Phys. Sci. 47 (1–2) (1992) 189.
[19] D. Sundholm, J. Olsen, Nuclear quadrupole moments of sulfur-33 and sulfur-35, Phys. Rev. A: At. Mol. Opt. Phys. 42 (3) (1990) 1160.

[20] G. Maciel, High-resolution nuclear magnetic resonance of solids, Science 226 (1984) 282.
[21] G.C. Chingas, K.T. Mueller, A. Pines, J. Stebbins, Y. Wu, J.W. Zwanziger, Dynamic-angle spinning of quadrupolar nuclei, J. Magn. Reson. 86 (1990) 470.
[22] S. Ganapathy, S. Schramm, E. Oldfield, Variable-angle sample-spinning high resolution NMR of solids, J. Chem. Phys. 77 (1982) 4360.
[23] E. Oldfield, R.J. Kirkpatrick, High-resolution nuclear magnetic resonance of inorganic solids, Science 227 (1985) 1537.
[24] K.T. Mueller, B.Q. Sun, G.C. Chingas, J.W. Zwanziger, T. Terao, A. Pines, Dynamic-angle spinning of quadrupolar nuclei, J. Magn. Reson. 86 (1990) 470.
[25] A. Samoson, A. Pines, Double rotor for solid-state NMR, Rev. Sci. Instrum. 60 (1989) 3239.
[26] E.W. Wooten, K.T. Mueller, A. Pines, New angles in nuclear magnetic resonance sample spinning, Acct. Chem. Res. 25 (1992) 209.
[27] L. Frydman, J.S. Harwood, Isotropic spectra of half-integer quadrupolar spins from bidimensional magic-angle spinning NMR, J. Am. Chem. Soc. 117 (1995) 5367.
[28] A. Medek, J.S. Harwood, L. Frydman, Multiple-quantum magic-angle spinning NMR: a new method for the study of quadrupolar nuclei in solids, J. Am. Chem. Soc. 117 (1995) 12779.
[29] M.J. Frisch, G.W. Trucks, H.B. Schlegel, G.E. Scuseria, M.A. Robb, J.R. Cheeseman, V.G. Zakrzewski, J.A. Montgomery, Jr., R.E. Stratmann, J.C. Burant, S. Dapprich, J.M. Millam, A.D. Daniels, K.N. Kudin, M.C. Strain, O. Farkas, J. Tomasi, V. Barone, M. Cossi, R. Cammi, B. Mennucci, C. Pomelli, C. Adamo, S. Clifford, J. Ochterski, G.A. Petersson, P.Y. Ayala, Q. Cui, K. Morokuma, N. Rega, P. Salvador, J.J. Dannenberg, D.K. Malick, A.D. Rabuck, K. Raghavachari, J.B. Foresman, J. Cioslowski, J.V. Ortiz, A.G. Baboul, B.B. Stefanov, G. Liu, A. Liashenko, P. Piskorz, I. Komaromi, R. Gomperts, R.L. Martin, D.J. Fox, T. Keith, M.A. Al-Laham, C.Y. Peng, A. Nanayakkara, M. Challacombe, P.M.W. Gill, B. Johnson, W. Chen, M.W. Wong, J.L. Andres, C. Gonzalez, M. Head-Gordon, E.S. Replogle, J.A. Pople, GAUSSIAN 98, Revision A.11.2 (Gaussian, Inc., Pittsburgh PA, 2001)..
[30] J. Skibsted, N.C. Nielsen, H. Bildsøe, H.J. Jakobsen, Satellite transitions in MAS NMR spectra of quadrupolar nuclei, J. Magn. Reson. 95 (1991) 88.
[31] J. Skibsted, N.C. Nielsen, H. Bildsøe, H.J. Jakobsen, Vanadium-51 MAS NMR spectroscopy: determination of quadrupole and anisotropic shielding tensors, including the relative orientation of their principal-axis systems, Chem. Phys. Lett. 188 (1992) 405.
[32] J. Skibsted, N.C. Nielsen, H. Bildsøe, H.J. Jakobsen, Magnitudes and relative orientation of vanadium-51 quadrupole coupling and anisotropic shielding tensors in metavanadates and potassium vanadium oxide (KV_3O_8) from vanadium-51 MAS NMR spectra. Sodium-23 quadrupole coupling parameters for a- and b-$NaVO_3$, J. Am. Chem. Soc. 115 (1993) 7351.
[33] T.C. Farrar, E.D. Becker, Pulse and Fourier Transform NMR, Academic Press, New York, 1971.
[34] M.H. Cohen, F. Reif, Quadrupole effects in nuclear magnetic resonance studies of solids, Solid State Phys. 5 (1957) 321.
[35] A.P.M. Kentgens, A practical guide to solid-state NMR of half-integer quadrupolar nuclei with some applications to disordered systems, Geoderma 80 (1997) 271.
[36] D. Freude, J. Haase, Quadrupole effects in solid-state nuclear magnetic resonance, NMR 29 (1993) 1–90.
[37] J. Haase, K.D. Park, K. Guo, H.K.C. Timken, E. Oldfield, Nuclear magnetic resonance spectroscopic study of spin–lattice relaxation of quadrupolar nuclei in zeolites, J. Phys. Chem. 95 (18) (1991) 6996.
[38] J. Haase, H. Pfeifer, W. Oehme, J. Klinowski, Logitudinal NMR relaxation of 27Al nuclei in zeolites, Chem. Phys. Lett. 150 (1988) 189.
[39] J. Haase, H. Pfeifer, W. Oehme, J. Klinowski, Longitudinal N.M.R. relaxation of aluminium-27 in zeolites is governed by quadrupole interactions with adsorbed polar molecules and exchangeable cations, J. Chem. Soc. Chem. Commun. 17 (1988) 1142.
[40] S.D. Jacobsen, J.R. Smyth, R.J. Swope, Rigid-body character of the SO4 groups in Celestine, anglesite and barite, Can. Miner. 36 (1998) 1053.
[41] A.A. Colville, K. Staudhammer, A refinement of the structure of barite from Cow Green Mine, Am. Miner. 52 (1967) 1877.
[42] American Mineralogist Crystal Structure Database. Available at: <http://www.geo.arizona.edu/AMS/>.
[43] S. Ahmed, A.M. Shamah, R. Kamel, Y. Badr, Structural changes of $(NH_4)_2SO_4$ crystals, Phys. Stat. Sol. A 99 (1987) 131.
[44] F.C. Hawthorne, R.B. Ferguson, Anhydrous sulphates. I. Refinement of the crystal structure of celestite with an appendix on the structure of thenardite, Can. Miner. 13 (1975) 181.
[45] K. Hasebe, Studies of the crystal structure of ammonium sulfate in connection with its ferroelectric phase transition, J. Phys. Soc. Japan 50 (1981) 1266.
[46] A.M. Abdeen, G. Will, W. Schaefer, A. Kirfel, M.O. Bargouth, K. Recker, A. Weiss, X-ray and neutron diffraction study of alums: III. The crystal structure of ammonium aluminum alum, Z. Kristallogr. 157 (1981) 147.
[47] S. Lidin, A.K. Larsson, A structural description of β-potassium sulfate, Acta Chem. Scand. 45 (1991) 856.
[48] A.C. Larson, D.T. Cromer, Refinement of the alum structures: III. X-ray study of the α-alums, K, Rb, and $NH_4Al(SO_4)_2(H_2O)_{12}$, Acta Crystallogr. 22 (1967) 793.
[49] D. Liu, H.M. Lu, J.R. Hardy, F.G. Ullman, Raman scattering and lattice-dynamical calculations of alkali-metal sulfates, Phys. Rev. B: Condens. Matter. 44 (1991) 7387.
[50] F. Hammel, Anhydrous sulfates of the magnesian series, Hebd. Seances Acad. Sci. 202 (1936) 57.
[51] F.C. Hawthorne, R.B. Ferguson, Anhydrous sulfates. II. Refinement of the crystal structure of anhydrite, Can. Miner. 13 (1975) 289.
[52] B.F. Pedersen, D. Semmingsen, Neutron diffraction refinement of the structure of gypsum, $CaSO_4(H_2O)_2$, Acta Crystallogr. B 38 (1982) 1074.